Insights into Ion Conduction Mechanisms Through the ORF3a Channel by Computational Modelling

Nuria Anguita-Ortiz[1(✉)], Andrea Lombardi[3,4(✉)], Noelia Faginas-Lago[3,4], and Juan J. Nogueira[1,2]

[1] Department of Chemistry, Universidad Autónoma de Madrid, Calle Francisco Tomás Y Valiente, 7, 28049 Madrid, Spain
{nuria.anguita,juan.nogueira}@uam.es
[2] IADCHEM, Institute for Advanced Research in Chemistry, Universidad Autónoma de Madrid, Calle Francisco Tomás Y Valiente, 7, 28049 Madrid, Spain
[3] Dipartimento di Chimica, Biologia e Biotecnologie, Università degli Studi di Perugia, 06123 Perugia, Italy
{andrea.lombardi,noelia.faginaslago}@unipg.it
[4] Istituto CNR di Scienze e Tecnologie Chimiche "Giulio Natta" (CNR-SCITEC), Via Elce di Sotto 8, Perugia 06123, Italy

Abstract. Investigating the selectivity and mechanism of the SARS-CoV-2 ORF3a protein channel remains a significant challenge within the scientific community. Speculation surrounds its potential calcium ion selectivity, implicating a significant role in the pathology of COVID-19 by influencing viral replication and the cellular virus response. This study employs molecular dynamics (MD) simulations with external electric fields to examine ion conduction, focusing on the interactions between calcium, potassium and sodium ions and specific amino acid residues in the ORF3a structure. Initial findings reveal a complex framework of conductance and selectivity, characterized by distinct patterns of residue coordination. These early insights underscore the channel's selectivity and functional mechanism, laying the groundwork for further in-depth studies aimed at unravelling the ORF3a protein's role in virus-host dynamics and its therapeutic potential. Advancements in ion-residue and ion-water coordination studies, along with extended molecular dynamics simulations, are essential to deepen our understanding and uncovering essential transport mechanisms that could be pivotal in designing effective antiviral compounds.

Keywords: Molecular Dynamics · Ion Conduction · Coordination · ORF3a

1 Introduction

The cells of living organisms are perpetually under the influence of physico-chemical environmental stimuli [1–3]. Considerable progress has been made in

© The Author(s), under exclusive license to Springer Nature Switzerland AG 2024
O. Gervasi et al. (Eds.): ICCSA 2024 Workshops, LNCS 14823, pp. 402–414, 2024.
https://doi.org/10.1007/978-3-031-65329-2_27

unraveling how cellular receptors directly link to intracellular electrochemical signaling. These receptors encompass a diversity of ion channels activated by voltage, ligands, or mechanical sensitivity, and are pivotal for cells to detect physical and chemical stimuli from the surroundings [4–6]. Among these stimuli, mechanical forces such as osmotic pressure, gravity, touch, fluid dynamics in contact with cells, and sound waves target various types of membrane proteins, triggering intracellular changes and leading to subsequent responses in the cell nucleus-a key aspect of the discipline of mechanobiology [7]. This intricate interplay between cells and their environment becomes critically relevant in the context of respiratory diseases, where the mechanobiological responses can influence disease progression and pathology [8,9].

Research on respiratory diseases, especially those caused by the coronavirus family, has been a crucial area of study in recent decades. The emergence of diseases such as Severe Acute Respiratory Syndrome (SARS), Middle East Respiratory Syndrome (MERS), and more recently, the global COVID-19 pandemic caused by SARS-CoV-2, has underscored the importance of advancing our understanding of these pathogens [10,11]. All these viruses belong to the Beta-coronavirus and have shown the ability to cause respiratory diseases of different severity in humans, which has accentuated the need for detailed research to develop effective prevention and treatments.

Within the coronavirus genome, a key element in their study is the presence of Open Reading Frames (ORF), which encode for the structural and non-structural proteins, essential for the replication and pathogenicity of the virus. ORFs are sequences of DNA or RNA that have the capacity to be translated into proteins, playing a crucial role in the virus's biology [1,8,12]. Among all, ORF3a is the largest accessory protein encoded by SARS-CoV-2 and has emerged as a protein of interest because it performs multiple roles in the virus life cycle and its implication in the pathology of the disease. The attributed functions include modulating the release of virions, inducing apoptosis in infected cells, and manipulating the host's immune response [8,9,11,13].

ORF3a has been classified as a viroporin, belonging to a class of transmembrane proteins that form ionic channels in cellular membranes [8,12,14], facilitating the flow of ions between the inside and outside infected cells, thus altering the intracellular ionic balance and promoting various pathological processes. The structure of this protein includes an N-terminal ectodomain, three transmembrane domains (TM1-TM3), and a cytoplasmic C-terminal domain, as observed in Fig. 1. This configuration facilitates its localization in the plasma membrane and the formation of ionic pores, fundamental aspects for its function in viral pathogenicity. It is believed that ORF3a acts as a non-selective channel permeable to cations, including calcium (Ca^{2+}), which has significant implications for viral replication as well as the induction of apoptosis in infected cells. In vitro experiments suggest that ORF3a could alter cellular calcium homeostasis, a finding that underscores the need to study its mechanism of action and selectivity [10,11,13–15]. In this contribution, we simulate the ion permeation through the

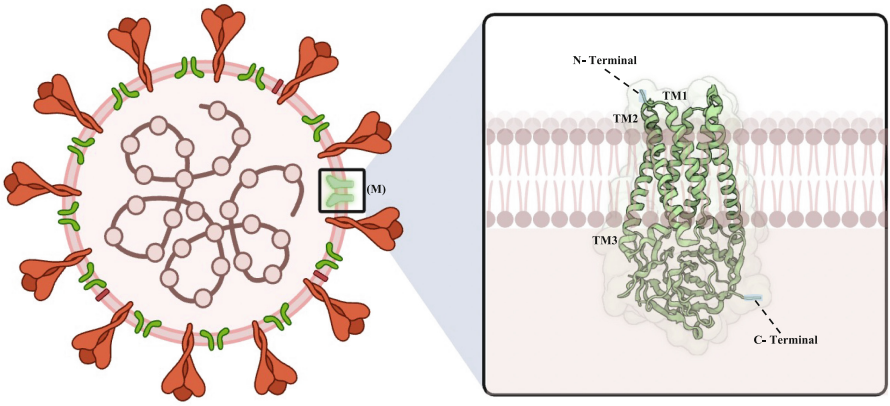


Fig. 1. Schematic structure of the ORF3a, a membrane protein (M) of the SARS-CoV-2 virus.

ORF3a channel by means of voltage-biased molecular dynamics simulations to unveil the most relevant protein residues involved in the conduction mechanism.

2 Computational Details

– **System Setup.** Protein coordinates were retrieved from the Protein Data Bank 7kjr entry [15], which delineates its structure as determined by cryo-electron microscopy at 2.1 Å resolution within a lipid environment [15]. An initial cleansing process was conducted using PyMol [16], aimed at removing all water molecules and residual ligands to purify the structure, leaving solely the ORF3a protein, thus ensuring its suitability for simulations. The preparation of the protein involved the adoption of the CHARMM36m force field [17], selected for its accuracy in modeling interactions between proteins and lipids in biomimetic contexts. Subsequently, with the assistance of CHARMM-GUI [18] and using the bilayer builder input generator [19], the protein was aligned along the Z-axis using the Orientations of Proteins in Membranes (OPM) database [20], before determining the dimensions of the simulation box. CHARMM-GUI follows a detailed procedure based on a set of parameters to define these dimensions. The process begins with the choice of a rectangular box. The length along the Z-axis is determined by the defined water layer thickness, set at 22.5 Å, which represents the minimum amount of water needed above and below the system. Dimensions along the X and Y axes are based on the lipid component ratios. The protein was then embedded in a pre-equilibrated DOPE (Dioleoylphosphatidylethanolamine) lipid bilayer, a phospholipid commonly found in biological membranes. DOPE lipid was chosen for both the upper and lower leaflets, leading to an initial estimate of the lengths of X and Y. As a result, the system was set up with dimensions of $60.288 \times 60.288 \times 127.277$ Å. Finally, to emulate physiological

conditions and maintain the system's neutrality, CHARMM-GUI automatically incorporates the necessary ions to neutralize the system (KCl is the usual choice). Additionally, specific ions of NaCl, KCl, and $CaCl_2$ were added up to a concentration of 150 mM to TIP3P water [21]. Once the system preparation was completed, NAMD inputs were generated and ready to launch the molecular dynamics simulation [22]. This simplified setup contains only one type of lipid, as this approach allows us to explore the fundamental mechanisms of ion transport and channel behavior without the computational costs associated with simulating a fully detailed lipid environment [4,5]. Such simplifications have been successfully employed in similar studies for prokaryotic voltage- activated sodium and potassium channels The generated simulation box is shown in Fig. 2.

– **Classical Molecular Dynamics**. After adjusting the default NAMD inputs provided by CHARMM-GUI, like modifications to enhance the thermal equilibration protocol, the heating process was subdivided into three distinct sequential stages. The system minimization was carried out using the conjugate gradient and line search method over 10,000 steps. Then, the system was progressively heated from 0 to 303.15 K in the NVT ensemble, using a time step of 1 fs during three distinct phases, the initial heating phase elevated the system from 0 to 100K, the second one from 100 to 200K, and the final stage reached 303.15k. This procedure, totaling 0.375 ns, allocated 0.125 ns for each phase. During the initial heating equilibration, the simulation was conducted within the NVT ensemble. Constraint scaling was initially set at 10.0kcal/(molA^2), subsequently adjusted to 5kcal/(molA^2), and then to 2.5kcal/(molA^2), applied to the alpha carbons of the protein to maintain its structural stability while allowing flexibility in other regions of the system. Temperature control was carried out using the Langevin thermostat [23], with a collision frequency of 1.0 ps^{-1}. Subsequent equilibration phases were conducted within the NPT ensemble, allowing for both temperature and pressure regulation, thereby facilitating system density adjustments. Constraints were sequentially reduced from 1, to 0.5, and finally, to 0.1kcal/(molA^2), before being completely removed (set to 0) for the production phase. Throughout these equilibration stages and the subsequent production phase, a consistent timestep of 2 fs was utilized, cumulatively amounting to an additional equilibration period of 1.5 ns. Pressure management was activated using the Langevin piston, configuring the system for pressure control through a Nose-Hoover Langevin piston [24]. A target pressure of 1.01325 bar, equivalent to 1 atmosphere, was established, with a piston oscillation period of 50 fs and an oscillation decay time of 25 fs. The Particle-Mesh Ewald (PME) method [25] was employed with a grid spacing of 1.0 Å for precise long-range electrostatic calculations, alongside a 12 Å cutoff and a 10 Å switching distance for nonbonded interactions to optimize computational efficiency and accuracy. The bonds containing hydrogen atoms were restrained using the SHAKE algorithm [26]. The first production phase, conducted in the NPT ensemble without an external electric field, lasted 100 ns, providing insights into the system's behavior under standard equilibrium conditions. Subsequently,

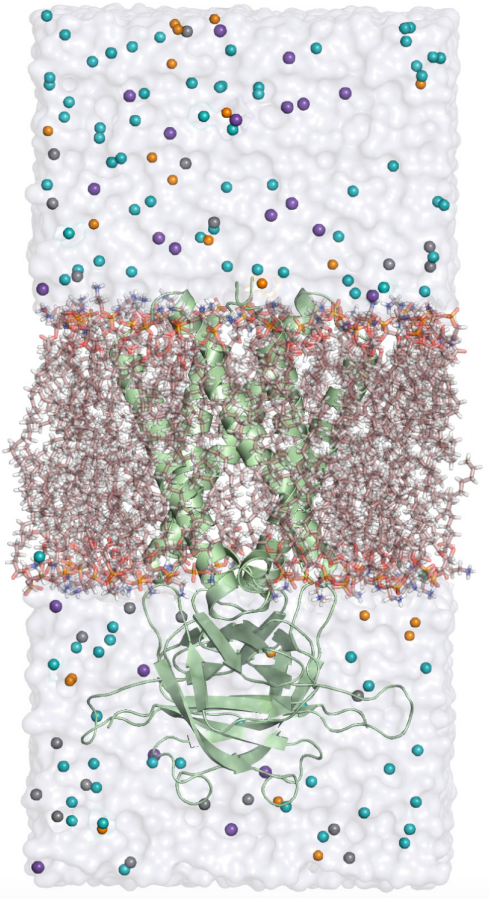


Fig. 2. The components of the simulation box. Protein is represented in green (cartoon), lipid bilayer in brown (licorice), chloride ion in cyan, sodium in orange, potassium in purple, and calcium in grey (spheres). Water is represented by the surface in light blue. (Color figure online)

a second production phase was evolved in the NPT ensemble, but this time incorporating an external electric field of 1.5 V in the Z direction (with the positive end towards the extracellular side, see Fig. 5) for another 100 ns. For a detailed explanation of the equations and their application in molecular dynamics, we recommend consulting the article [27], which is a standard reference in the field and provides a comprehensive description of the methodology and equations used. Moreover, the application of external electric fields in molecular dynamics has been previously utilized and is well described in the literature [28].

3 Results

In this section, a detailed analysis is carried out in two parts, aimed at getting insight into the mechanism of ion conduction and selectivity of the channel under study. The analysis is performed on the 100 ns production phase of the simulation, where an external electric field is applied, since it is during this stage that the ionic events occur. The application of this electric field induces an increase in the ionic mobility, which allows for the collection of a large amount of data, thus, facilitating a more accurate and rapid statistical analysis of the ion transport process. In the first part of the analysis, the ion permeation events are classified and counted for each ion type. Then, the second part of the analysis focuses on the identification of the aminoacids involved in the ion conduction by means of the characterization of the ion coordination sphere during the conduction events. Special attention has been given to negatively (GLU and ASP) and positively (LYS and ARG) charged amino acids for their ability to coordinate cations (sodium, potassium, and calcium) and anions (chloride), respectively. This analysis seeks to unveil the role of these coordinating residues on the reg-

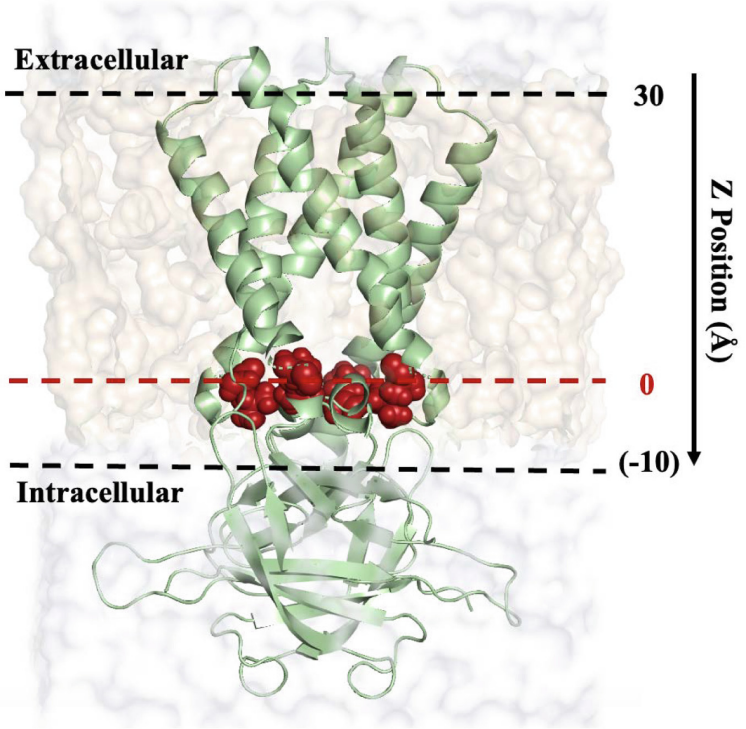


Fig. 3. Schematic representation of the transmembrane protein's orientation along the Z-axis.

ulation of ionic transport through the channel, providing valuable insights into the mechanisms underlying the channel's selectivity and efficiency.

To facilitate the understanding and visualization of the subsequent analyses, Fig. 3 presents a schematic representation of the orientation of the transmembrane protein with respect to the cellular bilayer along the Z-axis, which is the direction of the ion conduction. The extracellular and intracellular regions are differentiated by black dotted lines, while the zero reference point on the Z-axis is defined based on the geometric center of four reference amino acids, LEU 71 and ARG 126 from both chains A and B, depicted in the Fig. 3 as red spheres. The following analysis has been conducted with custom-developed Python programs, utilizing the MDAnalysis library.

– **Ion Conduction.** Figure 4 illustrates the ionic translocation events through the channel, depicted by colored dots moving from the extracellular region (Z=20 Å) to the intracellular region (Z=-20 Å). The examination of the plots reveals a higher number of conduction events for potassium ions (28) compared to sodium (17) and calcium (8). Despite the channel is supposed to be calcium selective, the simulation showcases significant activity for other cations. However, calcium events exhibit a more restricted and concentrated spatial distribution, as particularly observed in Fig. 4c around Z=10 Å, sug-

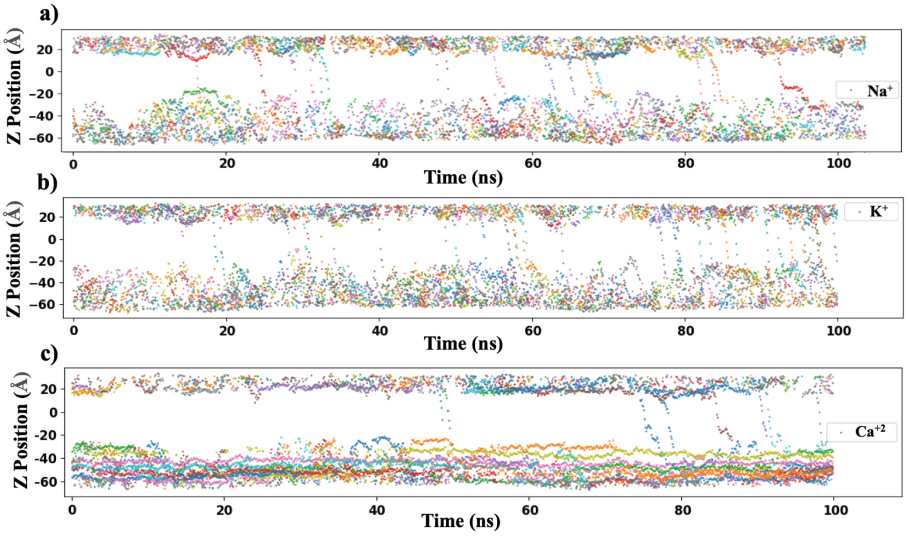


Fig. 4. Ion permeation profiles for **a)** $\mathbf{Na^+}$, **b)** $\mathbf{K^+}$ and **c)** $\mathbf{Ca^{2+}}$ along the Z-axis in Å over time in nanoseconds (ns).

gesting a potentially more specific and robust interaction with the protein. For instance, from approximately 25 ns to 40 ns, one can observe in purple that a calcium ion remains consistently in the same position, indicative of being retained. Additionally, the conduction of chloride ions was analyzed due to the observation of numerous events, but their graphical representation has been omitted. This decision was made because the individual events were not as discernible, with some occurring simultaneously or in rapid succession, as observed in simulation analysis software, in this case, PyMol.

– **Ion-Protein Coordination.** The coordination analysis elucidates the interactions between different residues and ions, providing relevant insight into their potential roles in the ion selectivity and mechanistic function of the channel. This analysis focuses on the interaction of different protein residues with calcium and the other cations, and their impact on channel dynamics. The residues that will strongly interact with the cations are the negative ones, i.e., glutamate and aspartate. Figure 5a and Fig. 5b show the coordination number of the different ions by glutamate and aspartate, respectively, with cutoff distances set at 2.5 Å for calcium, 3.0 Å for sodium, and 3.4 Å for potassium. These residues exhibit significant coordination with calcium ions and smaller coordination with sodium and potassium ions. This behaviour is likely due to the larger charge of calcium, which enhances the electrostatic interactions with the negative residues. Thus, glutamate and aspartate could be main actors in calcium conduction through the channels.

It is important to note the absence of coordination near the Z=0 point despite the presence of amino acids that might be crucial, suggesting alternative ion exit pathways from the channel or that the ions could be fully solvated by water in this region. Furthermore, positively charged residues, such as lysine and arginine displayed in Fig. 6a and Fig. 6b, respectively, show a strong coordination of the chloride anion (the cutoff distance was set at 2.5 Å), which indicate that the ion transport in this channel is a complex mechanism with different ions and residues involved. Further analysis are needed to investigate in more detail the mechanistic details. It should be noted that the coordination numbers for the ions involved in this study were determined based on the proximity of non-hydrogen atoms of the protein residues to the respective ions. Specifically, cutoff distances of 2.5 Å for calcium and chloride ions, and 3.0 Å and 3.4 Å for sodium and potassium ions, respectively, were employed. These distances correspond to the locations of the first minima observed in the ion-water oxygen radial distribution functions when the ions are in the bulk solvent.

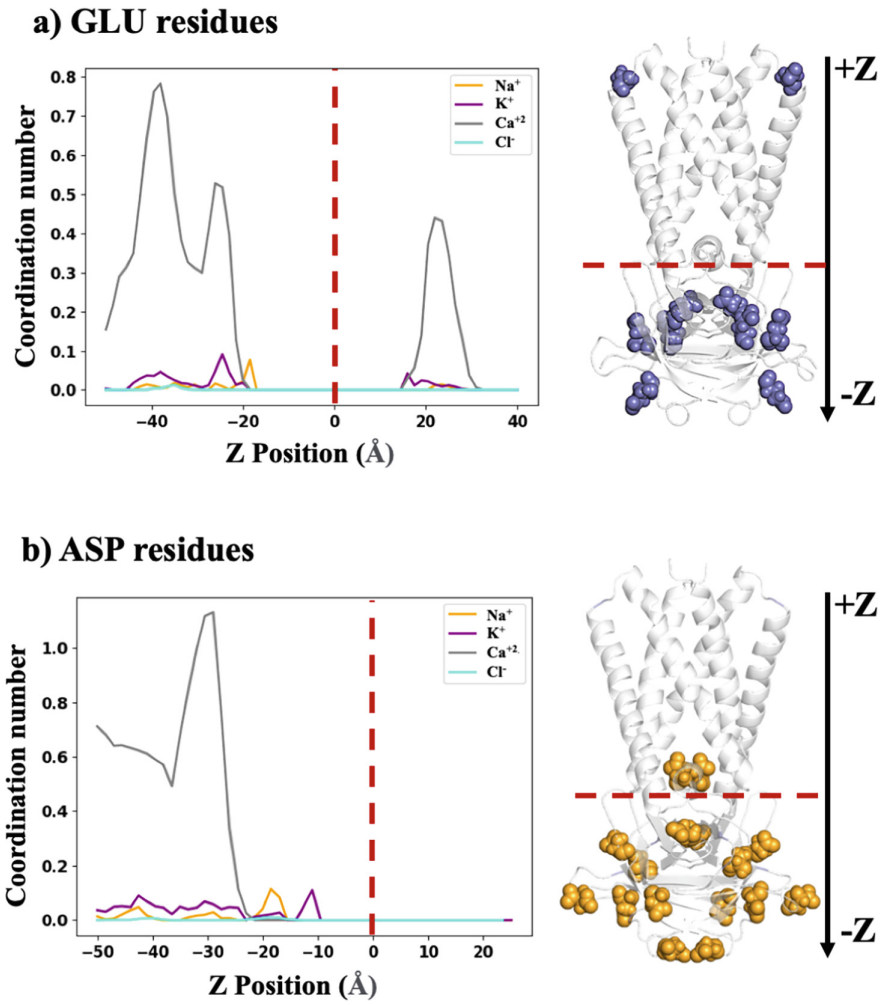


Fig. 5. Ion Coordination profiles for amino acids with negative charges along the Z-axis. **a)** GLU residues are denoted by blue spheres, **b)** ASP by orange spheres. The red dashed lines denote the zero reference point on the Z-axis. (Color figure online)

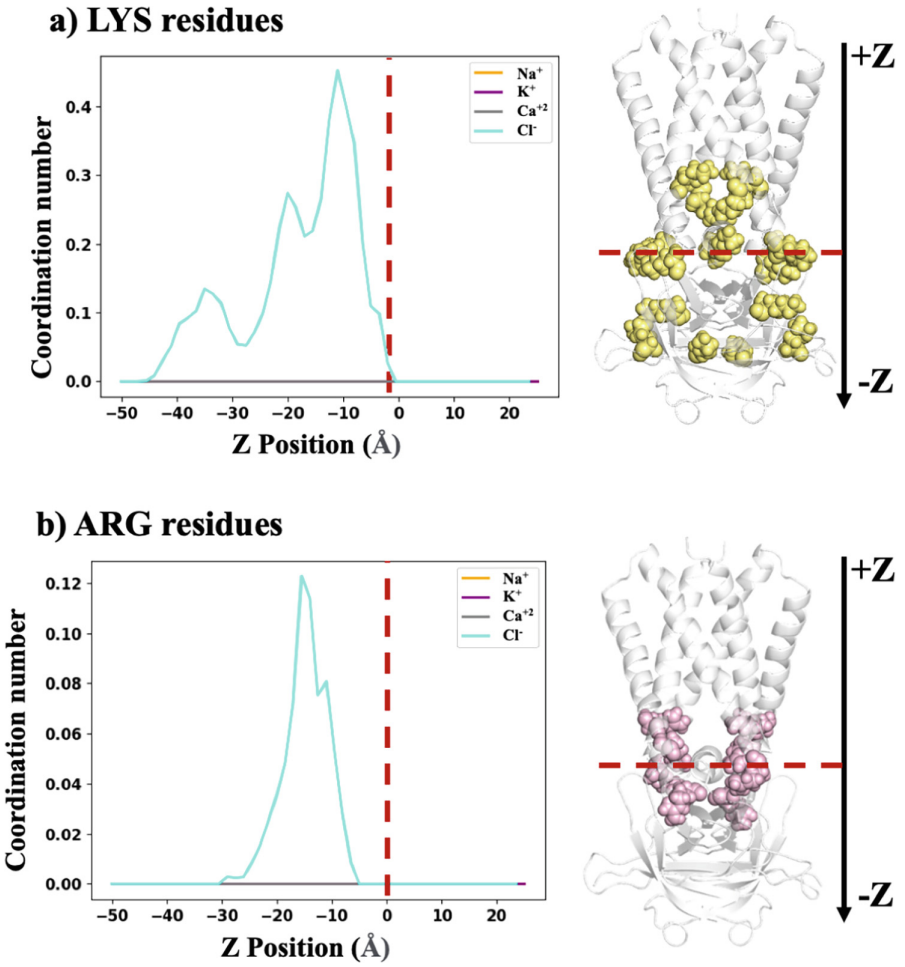


Fig. 6. Ion Coordination profiles for amino acids with positive charges along the Z-axis. **a)** LYS by yellow spheres, and **b)** ARG by pink spheres. The red dashed lines denote the zero reference point on the Z-axis. (Color figure online)

4 Conclusions

The analyses presented in this study offer a preliminary view of the ionic conduction dynamics through the ORF3a protein channel and its interaction with specific residues. The simulation has unveiled distinctive patterns in the conduction of calcium, potassium, and sodium ions, as well as coordination interactions with key residues within the protein. Specifically, the interaction between glutamate and aspartate residues with the calcium ions could be a key ingredient in the selectivity of this channel. Comparing this with the available experimental data [15], we find that, although the calcium conduction events are not predomi-

nantly high, the specific calcium coordination observed experimentally supports the selectivity and efficacy of this channel towards calcium, which is consistent with the significant coordination observed in our simulations. However, the permeation of other cations and anions and the coordination of chloride by positively charged amino acids suggest that the channel selectivity and conduction follow a very intricate mechanism that need a more thoughtful analysis and additional simulations.

The results presented here should be taken with caution due to the preliminary nature of the study. The simulations should be extended up to the microsecond timescale to enhance the statistical robustness and the reliability of the results obtained. Furthermore, it is recommended to increase the complexity of the system setup to be closer to real biological systems, even though this may entail a significant increase in computational cost. In addition, further analysis should also delve deeper into ion-water coordination and the interactions of ions with other amino acids (neutral ones) not considered in this initial analysis, but that could play a critical role in the ion conductance and selectivity of the channel. A more complete analysis based on longer simulations will allow us to unveil the factors that control the ionic dynamics through the ORF3a channel. Such relevant information will be crucial for the design of effective antiviral compounds.

Acknowledgements. The authors thank Atena Salek for preliminary calculations. We acknowledge the generous allocation of computer time at the Centro de Computación Científica at the Universidad Autónoma de Madrid (CCC-UAM). This work was partially supported by the Spanish Ministry of Science and Innovation through the project PID2020-117806GA-I00 and by the Comunidad de Madrid through the Attraction of Talent Program (Grant reference 2022-5A/BMD-24244). N. F-L and A. L thank the European Union - NextGenerationEU under the Italian Ministry of University and Research (MUR) National Innovation Ecosystem grant ECS00000041 - VITALITY - CUP J97G22000170005

References

1. Martinac, B., et al.: Cell membrane mechanics and mechanosensory transduction, pp. 83–141. Elsevier (2020). https://doi.org/10.1016/bs.ctm.2020.08.002, http://dx.doi.org/10.1016/bs.ctm.2020.08.002
2. Cox, C.D., Bavi, N., Martinac, B.: Bacterial mechanosensors. Annu. Rev. Physiol. **80**(1), 71–93 (2018). https://doi.org/10.1146/annurev-physiol-021317-121351, http://dx.doi.org/10.1146/annurev-physiol-021317-121351
3. Yu, Z.Y., et al.: Piezo1 is the cardiac mechanosensor that initiates the cardiomyocyte hypertrophic response to pressure overload in adult mice. Nature Cardiovasc. Res. **1**(6), 577–591 (2022). https://doi.org/10.1038/s44161-022-00082-0, http://dx.doi.org/10.1038/s44161-022-00082-0
4. Qiu, H., Shen, R., Guo, W.: Ion solvation and structural stability in a sodium channel investigated by molecular dynamics calculations. Biochimica et Biophysica Acta (BBA) - Biomembranes **1818**(11), 2529–2535 (2012). https://doi.org/10.1016/j.bbamem.2012.06.003, http://dx.doi.org/10.1016/j.bbamem.2012.06.003

5. Clark, M.D., Contreras, G.F., Shen, R., Perozo, E.: Electromechanical coupling in the hyperpolarization-activated k+ channel kat1. Nature **583**(7814), 145–149 (2020). https://doi.org/10.1038/s41586-020-2335-4
6. Nakayama, Y.: Corynebacterium glutamicum mechanosensing: From osmoregulation to l-glutamate secretion for the avian microbiota-gut-brain axis. Microorganisms **9**(1), 201 (2021). https://doi.org/10.3390/microorganisms9010201, http://dx.doi.org/10.3390/microorganisms9010201
7. Hamill, O.P., Martinac, B.: Molecular basis of mechanotransduction in living cells. Physiol. Rev. **81**(2), 685–740 (2001). https://doi.org/10.1152/physrev.2001.81.2.685, http://dx.doi.org/10.1152/physrev.2001.81.2.685
8. Zhang, Z., et al.: Structure of SARS-COV-2 membrane protein essential for virus assembly. Nature Commun. **13**(1) (2022). https://doi.org/10.1038/s41467-022-32019-3, http://dx.doi.org/10.1038/s41467-022-32019-3
9. Gorkhali, R., Koirala, P., Rijal, S., Mainali, A., Baral, A., Bhattarai, H.K.: Structure and function of major sars-cov-2 and sars-cov proteins. Bioinform. Biol. Insights **15**, 117793222110258 (2021). https://doi.org/10.1177/11779322211025876, http://dx.doi.org/10.1177/11779322211025876
10. Pezeshkian, W., et al..: Molecular architecture and dynamics of sars-cov-2 envelope by integrative modeling. Structure **31**(4), 492–503.e7 (2023). https://doi.org/10.1016/j.str.2023.02.006, http://dx.doi.org/10.1016/j.str.2023.02.006
11. Yan, W., Zheng, Y., Zeng, X., He, B., Cheng, W.: Structural biology of sars-cov-2: open the door for novel therapies. Signal Trans. Targeted Therapy **7**(1) (2022). https://doi.org/10.1038/s41392-022-00884-5, http://dx.doi.org/10.1038/s41392-022-00884-5
12. McClenaghan, C., Hanson, A., Lee, S.J., Nichols, C.G.: Coronavirus proteins as ion channels: current and potential research. Front. Immunol. **11** (2020). https://doi.org/10.3389/fimmu.2020.573339, http://dx.doi.org/10.3389/fimmu.2020.573339
13. Dolan, K.A., Dutta, M., Kern, D.M., Kotecha, A., Voth, G.A., Brohawn, S.G.: Structure of sars-cov-2 m protein in lipid nanodiscs. eLife **11** (2022). https://doi.org/10.7554/elife.81702, http://dx.doi.org/10.7554/eLife.81702
14. Bianchi, M., Borsetti, A., Ciccozzi, M., Pascarella, S.: Sars-cov-2 orf3a: mutability and function. Int. J. Biol. Macromol. **170**, 820–826 (2021). https://doi.org/10.1016/j.ijbiomac.2020.12.142, http://dx.doi.org/10.1016/j.ijbiomac.2020.12.142
15. Kern, D.M., et al.: Cryo-em structure of sars-cov-2 orf3a in lipid nanodiscs. Nature Struct. Molecular Biol. **28**(7), 573–582 (2021). https://doi.org/10.1038/s41594-021-00619-0, http://dx.doi.org/10.1038/s41594-021-00619-0
16. Schrödinger, LLC: The PyMOL molecular graphics system, version 1.8 (2015)
17. Huang, J., et al.: Charmm36m: an improved force field for folded and intrinsically disordered proteins. Nat. Methods **14**(1), 71–73 (2016). https://doi.org/10.1038/nmeth.4067, http://dx.doi.org/10.1038/nmeth.4067
18. Jo, S., Kim, T., Iyer, V.G., Im, W.: Charmm-gui: a web-based graphical user interface for charmm. J. Comput. Chem. **29**(11), 1859–1865 (2008). https://doi.org/10.1002/jcc.20945, http://dx.doi.org/10.1002/jcc.20945
19. Lee, J., et al.: Charmm-gui input generator for namd, gromacs, amber, openmm, and charmm/openmm simulations using the charmm36 additive force field. J. Chem. Theory Comput. **12**(1), 405–413 (2015). https://doi.org/10.1021/acs.jctc.5b00935, http://dx.doi.org/10.1021/acs.jctc.5b00935
20. Lomize, M.A., Pogozheva, I.D., Joo, H., Mosberg, H.I., Lomize, A.L.: Opm database and ppm web server: resources for positioning of proteins in membranes. Nucleic Acids Res. **40**(D1), D370–D376 (2011). https://doi.org/10.1093/nar/gkr703, http://dx.doi.org/10.1093/nar/gkr703

21. Mark, P., Nilsson, L.: Structure and dynamics of the tip3p, spc, and spc/e water models at 298 k. J. Phys. Chem. A **105**(43), 9954–9960 (2001). https://doi.org/10.1021/jp003020w, http://dx.doi.org/10.1021/jp003020w
22. Phillips, J.C., et al.: Scalable molecular dynamics on cpu and gpu architectures with namd. J. Chem. Phys. **153**(4) (2020). https://doi.org/10.1063/5.0014475, http://dx.doi.org/10.1063/5.0014475
23. Farago, O.: Langevin thermostat for robust configurational and kinetic sampling. Physica A: Statist. Mech. Appl. **534**, 122210 (2019). https://doi.org/10.1016/j.physa.2019.122210, http://dx.doi.org/10.1016/j.physa.2019.122210
24. Feller, S.E., Zhang, Y., Pastor, R.W., Brooks, B.R.: Constant pressure molecular dynamics simulation: The langevin piston method. J. Chem. Phys. **103**(11), 4613–4621 (1995). https://doi.org/10.1063/1.470648, http://dx.doi.org/10.1063/1.470648
25. Darden, T., York, D., Pedersen, L.: Particle mesh ewald: An nlog(n) method for ewald sums in large systems. J. Chem. Phys. **98**(12), 10089–10092 (1993). https://doi.org/10.1063/1.464397, http://dx.doi.org/10.1063/1.464397
26. Miyamoto, S., Kollman, P.A.: Settle: An analytical version of the shake and rattle algorithm for rigid water models. J. Comput. Chem. **13**(8), 952–962 (1992). https://doi.org/10.1002/jcc.540130805, http://dx.doi.org/10.1002/jcc.540130805
27. Adcock, S.A., MccCammon, J.A.: Molecular dynamics: survey of methods for simulating the activity of proteins. Chem. Rev. **106**, 1589–1615. https://doi.org/10.1021/cr040426m, http://dx.doi.org/10.1021/cr040426m
28. Gumbart, J., Khalil-Araghi, F., Sotomayor, M., Roux, B.: Constant elec- tric field simulations of the membrane potential illustrated with simple systems. Biochimica et Biophysica Acta (BBA) - Biomembranes **1818**(11), 294–302 (2012). https://doi.org/10.1016/j.bbamem.2011.09.030, https://doi.org/10.1016/j.bbamem.2011.09.030